CHAPTER ONE

PENNING TRAPS

Richard C. Thompson

Blackett Laboratory, Department of Physics,
Imperial College London, London SW7 2AZ, UK
r.thompson@imperial.ac.uk.

Penning traps have been in use for a wide range of experiments in mass spectrometry, plasma physics, atomic spectroscopy, quantum information, and quantum optics for over 40 years. In this chapter, we give an account of the principles of operation of Penning traps, together with a discussion of practical aspects of their use and their advantages for particular types of experiments. A brief survey of recent experiments using Penning traps demonstrates their wide applicability and continuing importance in many fields.

1. Introduction

A Penning trap confines the motion of charged particles by the use of static electric and magnetic fields. In essence, a quadrupole electrostatic field confines particles along a particular direction (the axis of the trap) and the magnetic field, which is parallel to this axis, confines their motion perpendicular to the trap axis. In this way, the particles are trapped in all three dimensions. The Penning trap can be used for electrons, positrons, or atomic and molecular ions, including highly-charged ions. The principles of its operation are straightforward and it has found application in a very wide range of areas of physics.

We start this chapter with a brief historical introduction to Penning traps, then we discuss the operating principles of the trap (Section 2). In Section 3, we introduce a rotating frame in which the behavior of the trapped particles can be visualized in an intuitive manner. We then discuss the particular advantages and disadvantages associated with the Penning trap, and illustrate some of these advantages with brief discussions of some relevant experiments (Section 4). We then look at various practical

aspects of the operation of the Penning trap (Section 5) including cooling techniques. In Section 6, we look in more detail at laser cooling in the Penning trap. Finally, we draw some overall conclusions about the Penning trap in Section 7.

The name "Penning Trap" was first introduced by Hans Dehmelt [1,2] in the early 1960s. He later received the Nobel Prize for his work with ion traps [3]. The trap was named after Franz Penning, who performed experiments in the 1930s on electric discharges between coaxial cylinders and noticed that the lifetime of the electrons was increased in the presence of an axial magnetic field [4]. Dehmelt used the Penning trap for radiofrequency (RF) spectroscopy of He^+ ions and demonstrated that the temperature of trapped ions could be measured by monitoring the induced current in an external circuit connected to the Penning trap electrodes (the so-called "Bolometric technique" [5]).

Other groups were also using Penning traps around the same time, for example, in Edinburgh, a Penning trap was used in the development of a source of polarized electrons [6]. In Mainz, measurements were made of the anomalous magnetic moment (i.e. the g-factor) of electrons in a trap [7,8], and an impressive precision of around three parts in 10^8 was obtained.

One of the most significant steps in the application of Penning traps in atomic physics was made in 1978 when laser cooling of trapped ions was first demonstrated [9]. This work also used the bolometric technique referred to above. Later experiments used fluorescence light for observing this process, as will be discussed later in this chapter.

2. Principles of Operation

2.1. *Motion of a single ion*

Charged particles interact strongly with both electric and magnetic fields and one attractive way to trap such particles would be to put them in a region where there is a three-dimensional (3D) minimum of the electrostatic potential, so that there is a force toward the center of the trap from all directions. However, this is disallowed by Earnshaw's theorem, which follows from the Poisson equation for the electrostatic potential ϕ in the absence of free charges, $\nabla^2\phi(x,y,z) = 0$. As a result, electrostatic fields can be used to trap along at most two axes, and in order to make a 3D trap, some other mechanism must be used to confine the motion in the remaining direction(s). One way of achieving this is to add a uniform magnetic field

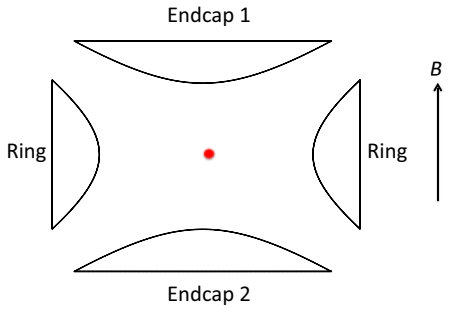

Fig. 1. Cross-section through the electrodes of a Penning trap. The two endcap electrodes are connected together. A DC potential applied between the endcaps and the ring creates a 3D quadrupole potential in the region between the electrodes. This traps particles along the vertical z-direction. The addition of a uniform magnetic field $\mathbf{B} = B\hat{\mathbf{z}}$ along the trap axis ensures 3D trapping. The separation of the endcaps is $2z_0$ and the internal diameter of the ring is $2r_0$, which is typically of the order of 1 cm (see text).

$\mathbf{B} = B\hat{\mathbf{z}}$ which can effectively confine the motion in the radial (x, y) directions by forcing the particle into circular orbits. If this is combined with a quadratic electrostatic potential,

$$\phi(x, y, z) = V_0(2z^2 - x^2 - y^2)/R^2, \tag{1}$$

a stable 3D trap is formed. Here V_0 is the applied trap potential and R^2 is a parameter related to the size of the trap. The potential described by this equation can be generated by a set of three electrodes having the cross-section shown in Figure 1, in which case R^2 is equal to $r_0^2 + 2z_0^2$, where r_0 and z_0 are the distances from the trap center to the ring and endcap electrodes, respectively. This potential has a saddle point at the center of the trap. Axial trapping is provided by the electric field of the saddle potential, which always provides a restoring force in the axial direction. Radial trapping is achieved with the help of the magnetic field, which provides an inward force for an orbiting particle that is stronger than the outward force in the radial plane arising from the saddle potential.

The equation of motion follows from the Lorentz force, $\mathbf{F} = m\ddot{\mathbf{r}} = e(-\nabla\phi + \mathbf{v} \times \mathbf{B})$, for a particle with mass m and charge e. The axial (z) motion then corresponds to simple harmonic motion (SHM) with an angular oscillation frequency $\omega_z = \sqrt{4eV_0/mR^2}$.

The equations of motion for the radial (x, y) motion are more complicated due to the presence of the magnetic field, which couples the two

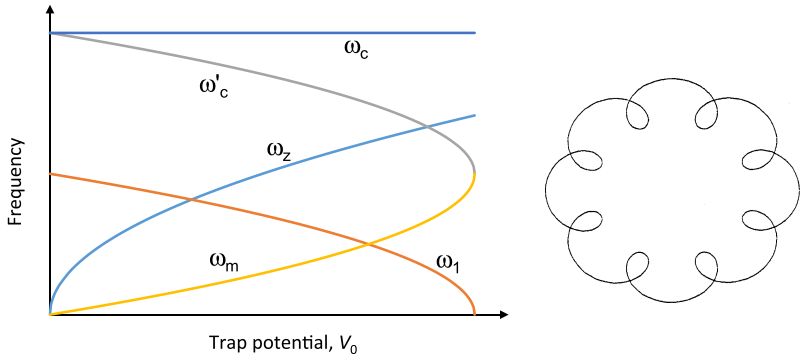

(a) (b)

Fig. 2. (a) Plot of the values of the various oscillation frequencies in the Penning trap as a function of the applied trap potential. (b) Typical radial orbit showing a small, fast cyclotron motion superimposed on a larger, slow magnetron orbit.

equations. However, by defining a complex variable $u = x + iy$, they can be combined in a single equation,

$$\ddot{u} - i\omega_c\dot{u} - (\omega_z^2/2)u = 0. \tag{2}$$

Here, $\omega_c = eB/m$ is the cyclotron frequency. The solution to the radial equation of motion is a superposition of two circular motions, one at the *modified cyclotron frequency*, $\omega_c' = \omega_c/2 + \omega_1$, and the other at the *magnetron frequency*, $\omega_m = \omega_c/2 - \omega_1$. The frequency ω_1 is equal to $\sqrt{\omega_c^2/4 - \omega_z^2/2}$ and we will see later that it has a simple physical interpretation.

The dependence of the trap oscillation frequencies on the applied trapping potential is shown in Figure 2(a). Note that all three trap oscillation frequencies (ω_z, ω_m, and ω_c') are always less than the cyclotron frequency ω_c and that the trap becomes unstable when the trapping potential is such that $\omega_z > \omega_c/\sqrt{2}$. At this point, the radial electric field, which pushes the ions away from the trap center, is strong enough to overcome the confining effect due to the magnetic field, so the ions are no longer confined radially. Figure 2(b) shows the path taken by an ion in the radial plane for the particular case that $\omega_c' = 9\omega_m$.

In many experiments (e.g. high precision mass spectrometry), it is necessary to find the value of the cyclotron frequency accurately. It can be seen that this is given by the sum of the magnetron and modified cyclotron frequencies, i.e. $\omega_c = \omega_m + \omega_c'$. However, this relation is exact only when the trap is perfect (that is, the potential is described exactly by Equation (1)).

It can be shown in Ref. [10] that the relation,

$$\omega_c^2 = \omega_c'^2 + \omega_z^2 + \omega_m^2 \tag{3}$$

remains exact even in the presence of misalignments and quadratic imperfections of the field. This equation can therefore be used to obtain accurate values of the cyclotron frequency for real traps that are not perfect.

It is worth noting here that although the axial motion is straightforward SHM, there are anomalies associated with the modified cyclotron and magnetron motions. As a result, the principle of equipartition of energy does not apply to these motions. The anomalies stem from the fact that the radial potential energy, given by $V = -\frac{1}{4}m\omega_z^2 r^2$, is negative, whereas in conventional SHM the potential energy is always positive. For the cyclotron motion, the kinetic energy, $K = \frac{1}{2}m\omega_c'^2 r_c^2$, which of course can only be positive, is always large enough to make the total energy of this motion positive. On the other hand, the kinetic energy associated with the magnetron motion, $K = \frac{1}{2}m\omega_m^2 r_m^2$, is smaller in magnitude than its potential energy, due to the low value of the magnetron frequency. Therefore, the total energy of this motion remains negative, and this has several consequences. One of the important consequences is that removal of energy from this motion results in an *increase* in the magnetron radius. So, if this motion is to be "cooled" (i.e. made smaller in amplitude), energy has to be supplied rather than removed. This means that cooling techniques have to be adapted for this motion.

2.2. *Interaction between ions*

If there are two ions present in the trap, the equations of motion are modified by including the force due to the Coulomb interaction, which introduces a term $e^2/4\pi\epsilon_0 r_{12}^2$, where r_{12} is the distance between the two ions. This couples the motion of both ions and also couples the x, y, and z motions. However, the new equations of motion can be separated into a *center of mass* motion and a *relative* motion. The center of mass motion is identical to that of a single ion, so the solutions are the same motions as we derived above. The relative motion depends on the Coulomb interaction and is no longer simple harmonic because of the nonlinear nature of the interaction. However, if the amplitude of the relative motion is small (i.e. if the temperature is low), a linear expansion of the Coulomb force can be made and the equations then become solvable.

There is a small number of types of motion that are of particular interest [11]. The first is when the two ions are both located on the trap axis at

locations $\pm z_1$, where $z_1^3 = e^2/16\pi\epsilon_0 m\omega_z^2$ (found by requiring the ions to be in static equilibrium). Then, the ions are essentially stationary apart from small oscillations due to the thermal motion of the center of mass motion and the relative motion (which for the axial direction can be shown to be at a frequency of $\sqrt{3}\omega_z$). Alternatively, the ions can be in equilibrium in the radial plane with a constant separation, but in this case, they are always moving in an orbit around the center of the trap. The separation can take different values, and this affects the frequency of the orbital motion. When the ions are well separated, they behave as if they are moving independently, so the frequencies of the relative motion approach the single particle values and the rotation around the trap center is generally close to ω_m. However, as the ions get closer together, the orbital frequency ω_R rises from ω_m to a value of $\omega_c/2$. At this point, the separation of the ions has its minimum value, which is $2r_1$, where $r_1^3 = e^2/16\pi\epsilon_0 m\omega_1^2$.

When there is a large number of ions in the trap, it becomes more appropriate to think of the motion in terms of a plasma rather than as individual particles. This type of plasma is referred to as a *single component plasma* or a *non-neutral plasma*. A detailed discussion of such a plasma is given in Chapter 9. Here, it is sufficient to note that at low temperatures, the plasma has an ellipsoidal shape with a constant number density n, a sharp edge and a well-defined aspect ratio. Due to the presence of the magnetic field, the whole plasma rotates at a frequency ω_R, where ω_R is related to n through

$$n = 2\epsilon_0 m\omega_R(\omega_c - \omega_R)/e^2. \tag{4}$$

In a manner similar to the case of two ions, when the ions have large separations (i.e. for low n), the value of ω_R is approximately ω_m, but when the ion density takes its maximum possible value, ω_R becomes equal to $\omega_c/2$. This situation, when the plasma density is maximum, is referred to as *Brillouin flow*.

3. Rotating Frame

We now show that the dynamics discussed above can be understood in a more intuitive manner by moving into a frame of reference that is rotating at $\omega_c/2$ [11]. The equations of motion for a single ion in a rotating frame acquire additional terms due to the centripetal force and the Coriolis force. However, by choosing the rotation frequency to be equal to $\omega_c/2$, the centripetal force exactly balances the Lorentz force due to the magnetic field,

and this simplifies the equations of motion considerably. In particular, it removes the coupling between the x and y motions, so each becomes SHM at a new frequency which is dependent on the effective potential resulting from the centripetal force. This oscillation frequency takes the value $\sqrt{\omega_c^2/4 - \omega_z^2/2}$ and it will be seen that this is identical to the value of ω_1 given above. The radial motion of a single ion in a Penning trap can therefore be interpreted as motion in a two-dimensional (2D) simple harmonic potential well (with an oscillation frequency ω_1) in a frame which is rotating at $\omega_c/2$ relative to the laboratory frame. An orbit at a frequency $+\omega_1$ in the rotating frame corresponds to the modified cyclotron motion ($\omega_c' = \omega_c/2 + \omega_1$) in the laboratory frame, while an orbit at $-\omega_1$ corresponds to the magnetron motion ($\omega_m = \omega_c/2 - \omega_1$) in the laboratory frame.

This simple way of interpreting the motion of a single ion also applies in the case of two ions and in the case of a large ion plasma. Consider the motion of two ions in a radial potential characterized by an oscillation frequency ω_1. The ions experience a Coulomb interaction as well as the force from the confining potential. However, when the ions are far apart, the Coulomb interaction is very weak and therefore, they behave essentially independently, so they both move at the single ion frequency in this frame, ω_1. If, on the other hand, the ions are stationary in the rotating frame, they will be in equilibrium close to the minimum of the potential, with a separation $2r_1$ where $r_1^3 = e^2/16\pi\epsilon_0 m\omega_1^2$, so the outward Coulomb force on each ion is exactly balanced by the inward force due to the confining potential. When this arrangement is viewed from the laboratory frame, the ions will be rotating at $\omega_c/2$ as we discussed above.

Similarly, the limits of low and high ion density for a plasma containing many ions can be treated simply in this rotating frame. The general case is when a uniform density plasma is rotating as a solid body at a rate ω_R' in the rotating frame. If the ions were stationary in that frame ($\omega_R' = 0$), they would have a density,

$$n = m(\omega_z^2 + 2\omega_1^2)\epsilon_0/e^2 = m\omega_c^2\epsilon_0/2e^2. \tag{5}$$

If however the plasma is rotating at ω_R', each ion experiences an additional outward centrifugal force due to the rotation, which is equal to $m\omega_R'^2 r$, and reduces the inward force from the trapping potential, $m\omega_1^2 r$. This is equivalent to a reduction of the trap oscillation frequency from ω_1 to $\omega_2 = \sqrt{\omega_1^2 - \omega_R'^2}$. If we substitute this new value into the expression for n, Equation (5), we obtain the new value for the number density,

$$n = m(\omega_z^2 + 2\omega_2^2)\epsilon_0/e^2 = 2m\omega_R(\omega_c - \omega_R)\epsilon_0/e^2. \tag{6}$$

This is identical to the general expression for the number density in the Penning trap, Equation (4), so the variation of number density with plasma rotation frequency can simply be seen as the consequence of the centrifugal force in the rotating frame.

4. Advantages of Penning Traps

In this section, we discuss several features of Penning traps that make them particularly suitable for certain types of experiment. We also show how these advantages are exploited in particular experiments.

4.1. *Isolated and stable environment*

Ions in any type of ion trap are well isolated from their environment: their motion is confined to a particular region by the use of electromagnetic fields, so there are no collisions with the walls of the container. Also, trapping is generally carried out under ultrahigh vacuum (UHV) conditions, so there are no collisions with background gas either. Although ions can collide with each other, their mutual Coulomb repulsion means that they never get close to each other and the internal electronic state is not affected by collisions, and the same is even true for the rotational and vibrational states of trapped molecular ions.

In a Penning trap, the confining fields are static, so there is no micromotion (which can lead to heating) as it occurs in the case of RF traps (see Chapter 2). This means that 3D plasmas containing many thousands of ions can be held under stable conditions in which there are no significant heating effects.

The nature of the confinement in the Penning trap means that ions are isolated from many perturbations and this allows various types of experiment to be performed that are otherwise not possible. For example, a microwave frequency standard based on a cloud of laser-cooled Be^+ ions in a Penning trap was able to achieve very long interaction times, which in turn gives narrow line-width and high frequency stability. In one experiment, Ramsey fringes were observed with an interaction time of 550 s, which gives a central fringe width of only 1 mHz on a transition frequency (between Zeeman states of the hyperfine structure of the ion) of around 300 MHz [12]. Of course, one potential problem with an experiment like this is the unavoidable presence of the magnetic field because any fluctuations of the magnetic field strength will lead to frequency shifts of the transition being studied. However, it is often possible to find a magnetic

field at which the RF becomes independent of field to first order, and this allows the effect of magnetic field fluctuations to be strongly suppressed.

An extreme example of the advantage of isolation of trapped particles in a Penning trap is the use of trapped antiprotons and trapped positrons to create antihydrogen. Storage and accumulation of antiparticles would be impossible in other systems because as soon as the particles encounter normal matter, they will annihilate. Therefore, positrons and antiprotons are both routinely stored in Penning traps in the experiments to create and study antihydrogen carried out at the CERN antiproton decelerator. Complex arrangements in these experiments are used to trap both species in the same trap structure, which consists of a long string of cylindrical electrodes with independently-controllable potentials. Regions designed to trap the positively charged positrons have a potential minimum, whereas regions for antiproton storage have a potential maximum. Using careful control of the potentials on each electrode, these regions can be overlapped in order to merge the clouds of positrons and antiprotons for the creation of antihydrogen (see Chapter 14).

4.2. *Tight localization of a single particle*

When a single atomic ion is held in a Penning trap and laser cooled, the typical temperature achieved (the Doppler limit) is around 1 mK. For standard trapping parameters, the residual thermal motion at this temperature is confined to a region having dimensions of the order of 1 μm. This opens up the possibility of very long interaction times between an ion and a laser beam, knowing that the ion will be within the laser beam the whole time and that the Doppler effect due to the residual motion of the ion will be very small. Thus, many delicate experiments have been performed where a single particle is observed continuously — for example in the observation of quantum jumps, where an ion jumps between two electronic levels, one of which interacts resonantly with the Doppler cooling laser, and therefore emits a continuous stream of fluorescence, while the other is 'dark'. When the ion is in this state, it does not interact with the laser and therefore, there is no fluorescence.

4.3. *Strong magnetic field*

Penning traps always involve the application of a strong magnetic field, typically of the order of a few tesla and usually provided by a superconducting magnet. In some cases, this is a disadvantage — for example,

the resulting Zeeman splitting of energy levels in laser cooling experiments may lead to the requirement to have more laser frequencies available — but for some experiments, it is a distinct advantage. This is particularly true for measurements of mass and of magnetic moments (see Chapter 17).

For the measurement of mass to high precision, it is convenient to measure the cyclotron frequency in a magnetic field because the cyclotron frequency is directly related to the mass ($\omega_c = eB/m$) and if the field is uniform and stable, it is possible to obtain high precision. There are therefore many examples of experiments that give very precise mass measurements using Penning traps. They are often used at facilities where a wide range of isotopes (including short-lived radioactive isotopes) can be produced, e.g. ISOLTRAP at the CERN ISOLDE facility [13]. In practice, mass measurements are made by a comparison of the cyclotron frequency of the particle of interest to that of a particle whose mass is already well known. If these measurements are made in the same magnetic field, the ratio of the masses is equal to the ratio of the cyclotron frequencies. The pure cyclotron frequency is determined from measurements of the three center of mass modes and combined using Equation (3). Accuracies of better than one part in 10^8 are achievable even for short-lived isotopes. These measurements are important because they allow the determination of nuclear binding energies for a wide range of isotopes, which is necessary for the understanding of nuclear structure physics. For the highest accuracy, a single particle is used and many repeated measurements are made. The proton mass has been determined this way to a precision approaching one part in 10^{10} [14].

Mass spectrometry to lower precision is carried out routinely in a technique known as *Fourier Transform Ion Cyclotron Resonance* (FT-ICR) [15]. This is essentially based around the measurement of the cyclotron frequency of molecular ions in a Penning trap, but it can be used not just for one species but for the analysis of samples containing many different species. The basic design of the 'cell' is similar to a Penning trap, but there is often no attempt made to design the electrodes to match the ideal quadrupolar shape closely. The analysis is performed by radially exciting the sample held in the cell and then taking the Fourier transform of the signal induced in an external circuit resulting from the motion of the ions after excitation. The Fourier transform yields a mass spectrum directly.

In order to measure a magnetic moment, it is necessary to compare the cyclotron frequency of a particle with its spin flip frequency in the same magnetic field. For an electron, these two frequencies are very close

because the spin flip frequency ω_s is equal to $g\mu_B B/\hbar = geB/2m$, where the gyromagnetic ratio of the electron $g = 2.00232$. The occurrence of spin flips is detected by introducing a quadratic variation of magnetic field strength with axial position. This changes the axial oscillation frequency slightly for the two different orientations of the spin of the particle, allowing its spin direction to be determined. In this way, the electron's gyromagnetic ratio has been determined to better than one part in 10^{12} [16]. This gives an accurate test of the theory of quantum electrodynamics (QED), which predicts a value of g to high precision given the value of the fine structure constant α.

The magnetic moments of other particles can also be measured in a Penning trap. For instance, the magnetic moment of the proton has recently been measured to very high precision [17]. This experiment, which reaches a precision of around three parts in 10^9, is much more difficult than the electron experiment because the magnetic moment is so small, and this means that a much stronger variation of magnetic field is necessary, which in turn requires that in order to obtain high precision, the excitation of the spin flip and the detection of the spin state of the particle have to be carried out in different locations. There is currently much interest in applying the same technique to measure the magnetic moment of the anti proton. This would allow a comparison of the g-factor of the proton and antiproton to be carried out, which can serve as a test of CPT invariance — one of the most fundamental symmetries in physics. This comparison has already been carried out at the level of 1 ppm (10^{-6}) [18], but the latest measurement techniques should allow a comparison at a level approaching 1 ppb (10^{-9}).

So far, we have only discussed the magnetic moment of free particles. However, the magnetic moment of particles in a bound system is also of interest. In particular, the magnetic moment of an electron in an atomic system is affected by the presence of the nucleus and again, this can be used to perform a test of QED calculations for a bound state (as opposed to the case of a free particle). For these experiments, a similar technique to that described above is used. An example is the measurement of $^{16}O^{7+}$, i.e. a single electron bound to an oxygen nucleus (also known as hydrogen-like oxygen) [19]. In this experiment, the g-factor was measured to a precision of around 3 ppb, consistent with bound state QED calculations. The deviation from the free particle value increases with the nuclear charge (Z) and so measurements in high-Z systems allow the higher-order terms in the QED calculation to be tested.

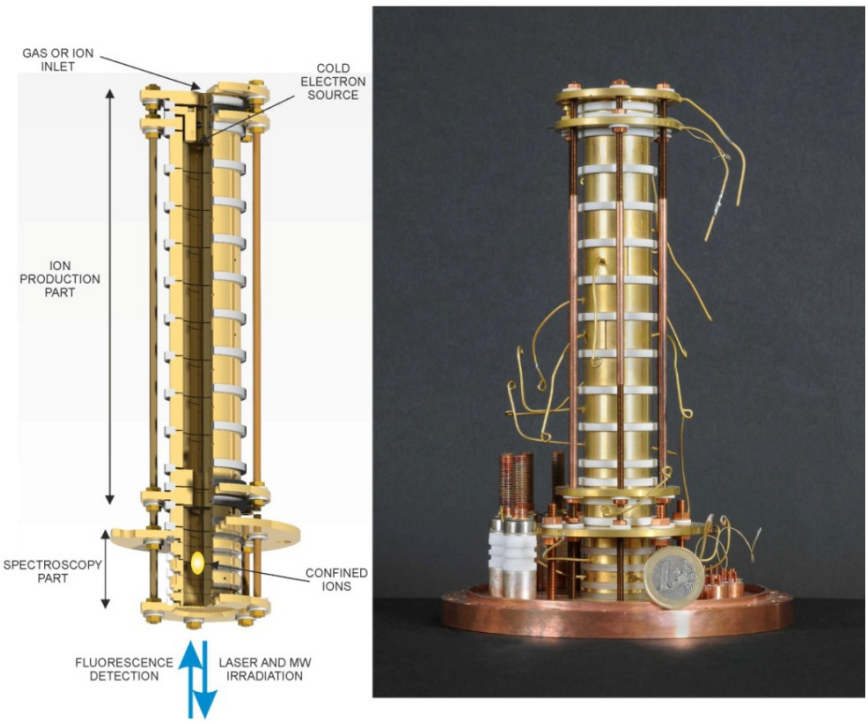

Fig. 3. Cutaway drawing (left) and image (right) of the ion trap for the ARTEMIS experiment at GSI in Darmstadt. The cylindrical electrodes can be configured to give trapping potentials at different locations in the magnetic field. Figure reproduced with permission from GSI.

An example of a trap designed for experiments in this area is shown in Figure 3. The trap is held at cryogenic temperatures when inside the superconducting magnet. The gold-plated hollow cylindrical electrodes can be configured to give trapping potentials at different locations in the axial magnetic field in order to move the ions around. The trap is designed for the measurement of the g-factors of medium to heavy hydrogen-like highly charged ions such as $^{28}Si^{13+}$ [20].

4.4. *Cooling of ions*

The ability to cool particles in traps is one of their major advantages over other techniques such as the use of gases, plasmas or atomic beams. Not only is it possible to cool trapped particles, but because they are well isolated from the environment, there is very little unwanted heating, so once

they are cooled, the particles will generally remain cold for a long time. There are several different cooling techniques, the most important techniques for Penning traps being laser cooling (discussed in Chapter 6) and resistive cooling (discussed along with other non-laser cooling techniques in Chapter 7). Radiative cooling via synchrotron radiation is also possible but that only applies to the cyclotron motion of electrons or positrons, so it is not discussed any further here.

4.4.1. *Resistive cooling*

In resistive cooling, the motion of ions in the trap gives rise to the induced flow of current in an external electrical circuit and hence to dissipation of energy which comes originally from the motion of the ions (see Chapter 7). An equilibrium is reached where the temperature of the ions is equal to that of the external circuit. If the trap and electronics are at cryogenic temperatures, this means that the temperature of the ion motion can also be in this region. In general, resonant circuits are used, where the trap itself forms part of the circuit and is connected in such a way that it is sensitive to either the axial or the radial motion of the ions. The resonant frequency of the circuit is chosen to coincide with the corresponding oscillation frequency. Although the axial and modified cyclotron motions can be cooled very effectively using this technique, the magnetron motion cannot be cooled this way because the extraction of energy leads to an *increase* of the size of the orbit. The magnetron motion therefore has to be cooled in a different way. Often, this is done by coupling the magnetron motion to the modified cyclotron motion with an applied field oscillating at their sum frequency (ω_c). This can be shown to give rise to a reduction in the size of the orbits of both motions when the modified cyclotron motion is subject to resistive cooling. This technique is called *axialization* [21] or *radial centering*. Resistive cooling is very effective for all species of trapped particles, but it is limited to the temperature of the apparatus, so it is not possible to cool to lower than a few K in general. It is used extensively in precision experiments on trapped ions.

4.4.2. *Laser cooling*

In laser cooling, momentum is exchanged between a laser beam and the ions. Laser cooling of trapped ions is discussed in Chapter 6 (see also, for example, [22]). This technique is only applicable to a small number of species of atomic ion because it needs a suitable atomic energy level structure including a strong optical transition from the ground state of the

ion to an excited state which mainly decays back to the ground state. Any other state to which the ion can decay needs to be emptied with a separate laser to return the ion into the laser cooling cycle. In a Penning trap, it is most convenient to work with a system that has no other states into which the ion can decay as otherwise the Zeeman splitting of the states leads to a requirement for many separate laser frequencies. Magnesium and beryllium are the only species where a single laser is required.

The simplest type of laser cooling is *Doppler cooling*, where the Doppler effect is used to make the interaction with the laser stronger when the ion is moving towards the laser and weaker when it is moving away from the laser. This is achieved by tuning the laser slightly to the lower frequency (red) side of the ion's transition frequency. Each time the ion absorbs a photon from the laser, it slows down slightly. The limiting temperature, referred to as the Doppler limit, is determined by a balance between this cooling process and heating that arises from the random nature of the re-emission of photons when the ion decays back to its electronic ground state from the excited state. The Doppler limit is given by $T_D = \hbar\gamma/k_B$ where γ is the decay rate of the excited state. Typically, the Doppler limit for ions of interest is in the range of 1 mK. Laser cooling in the Penning trap, is complicated by the unstable nature of the magnetron motion and we discuss it in more detail in Section 6.

The advent of Doppler laser cooling has had an enormous impact on the range of experiments that is possible in Penning traps (and of course in RF traps too). Doppler cooling effectively eliminates the Doppler effect and reduces the amplitude of the motion of ions so much that they are nearly stationary in the trap (except that in the Penning trap, a cloud of ions will always rotate due to the presence of the magnetic field, even when the ions are cold).

In order to achieve the lowest temperatures, it is necessary to use *optical sideband cooling*. In this cooling technique, the quantum mechanical nature of the motion of an ion in the trap is addressed directly. It is possible to cool the ion to the ground state of its motion. This requires a more complicated energy level structure than simple Doppler cooling, and in particular, it requires a metastable state to be available. Sideband cooling is also discussed in more detail in Section 6.

4.4.3. *Sympathetic cooling*

Sympathetic cooling is a way of extending some of the advantages of Doppler laser cooling to other species that cannot themselves be laser

cooled. It works by trapping a mixture of two species at the same time. If one of them is cooled directly using laser cooling, it will also bring down the temperature of the other species through exchange of energy in thermal collisions. Eventually, both species will end up at an equilibrium temperature close to the Doppler limit [23].

4.5. *Disadvantages of the Penning trap*

There are of course disadvantages to the use of Penning traps as well as advantages. The most important one is probably the need to provide a strong magnetic field. This generally involves the use of a superconducting magnet. These are expensive to buy and expensive to run due to the need for a continual supply of liquid helium and liquid nitrogen. Furthermore, since the size of the bore of the magnet is usually a limitation, access to the ions is generally difficult, especially if optical access for lasers and fluorescence is required. Even using optimized designs for the trap electrodes, they will restrict the access to the trapped particles. Once the trap is installed in the magnet, it is generally not possible to make mechanical adjustments, so mirrors and lenses need to be adjusted beforehand such that they cannot go out of adjustment when the trap is installed in the magnet. The need for UHV conditions further complicates access.

Since a vacuum of at least 10^{-9} mbar is required, strong pumping and very careful preparation of the trap components are necessary if the trap is to be held at room temperature (see Chapter 5). If the trap itself is to be held at cryogenic temperatures (as is the case for many experiments, for example, those measuring the magnetic moments of elementary particles and ions), an extremely good vacuum should be attained easily as any cryogenic surface can effectively act as a pump. However, the design of a cryogenic system adds its own complications due to the need for low heat conductance to the outside world.

Finally, the characteristics of the magnetron motion lead to several complications in the use of the Penning trap. Any collisions with residual gas in the vacuum chamber will lead to an increase of the radius of this motion, so the requirement for UHV conditions is particularly strong for the Penning trap. Also, laser cooling needs to be modified for the magnetron motion and even then the cooling rate for this motion is relatively slow. For an ion cloud in a Penning trap, the equivalent of the magnetron motion is a rotation of the whole cloud, so there is always some residual motion even when the temperature is very low. This also causes complications in some experiments.

5. Practical Aspects

5.1. *Design of Penning traps*

The design of a Penning trap is generally determined by the type of experiment it is to be used for. Most Penning traps are designed for use in a superconducting magnet, so the access to the trap is generally along the bore of the magnet and will be constrained by the size of the bore, typically 10 cm in diameter. The electrodes need to be designed to give a pure quadrupole potential near the center of the trap. Although the ideal shape for Penning trap electrodes is therefore a hyperboloid of revolution with a cross-section as shown in Figure 1, this shape is difficult to manufacture accurately and gives very poor access. However, it has been shown in Ref. [24] that a trap consisting of a set of cylindrical electrodes can be designed such that a very good quadrupole field can be generated by careful choice of the length of each electrode. This principle has been used in many traps and it has several advantages including ease of manufacture, good access along the trap axis, and good control of the higher-order terms in the trapping field.

This type of design can also be adapted to the situation where ions need to be moved between different trapping zones (for example, where ions are prepared in one trapping zone but detected or probed in another). In this case, the trap assembly may have tens of electrodes which can be configured in different ways to move ions around (see, for example, Figure 3).

In contrast to experiments that aim to provide a pure quadrupole potential, many studies that focus on the properties of non-neutral plasmas require a large trapping volume and it may not be important for the potential to be accurately quadratic. The electrodes are also usually cylindrical in this case. The central ring electrode may then be relatively long with shorter endcaps providing axial confinement of a plasma that adopts a long, thin shape like a cigar (a prolate ellipsoid). This type of trap is generally referred to as a Penning–Malmberg trap. For more details, see Chapter 9. Similarly, in the case of FT-ICR, the trap or cell may be constructed from electrodes with a simple geometry without causing problems for the use of the technique.

5.2. *Loading of ions into the trap*

If atomic ions are to be trapped, they can be created inside the trap or transported into the trap from outside. Creation of ions in the trap can be performed by forming a low-pressure vapor of the species to be ionized (e.g.

from a small atomic oven that is heated resistively) and ionizing them either by electron impact (using an electron beam that travels along the magnetic field line from a filament or some other source) or by photo-ionization using a pulsed or cw laser. The advantage of using photo-ionization is that the process can be made resonant, so it is then more selective, and unwanted ions will not be created. An alternative in-trap loading technique is direct ablation of ions from a surface using a pulsed laser.

Ions can also be created outside the trap and guided into it along the magnetic field lines. This is more appropriate for ions created in an accelerator (especially rare isotopes or highly-charged ions) and also for other particles such as electrons or protons. One point to note with externally-created ions is that if they have sufficient energy to enter the trap, they will also have sufficient energy to leave the trap again, so something has to be done to ensure that they stay in the trap. One way to do this is to lower the potential on one endcap to let the ions in and then to raise it again immediately so that when they reflect off the potential on the other endcap, they will no longer be able to leave the trap.

5.3. *Detection of ions*

In the Penning trap, the most common techniques are fluorescence detection, electronic detection or direct (destructive) detection of the charged particles. See Ref. [25] for a wider discussion of detection techniques for trapped ions.

Fluorescence detection is used in experiments where laser cooling is employed. It is a very sensitive detection technique and allows a single particle to be detected with ease once it is cold. Fluorescence levels of tens of thousands of counts per second can be obtained under ideal conditions, but the optical access issues mentioned above need to be dealt with carefully.

Electronic detection is strongly related to resistive cooling as both rely on the use of an external circuit that is resonant with the frequency of oscillation of the ions in the trap. Since resistive cooling dissipates energy via an induced current in the external circuit, detection of the ions is possible by monitoring the current in the circuit. This is used extensively in experiments on single electrons, protons and ions where a sensitive detection of the response of the particle to an external drive is required. In general, the electronic detection circuit for single particles needs to be held at cryogenic temperatures so that the required signal can be detected above the thermal noise.

Finally, direct detection of ions is possible on a microchannel plate (MCP) detector. If ions are released from the trap, they will always travel along the magnetic field lines in a cyclotron motion, so this can be used to guide all the ions to the detector. However, this destructive technique is not ideal because it means that the creation and preparation of the ions has to be repeated many times and this may be a lengthy process. In some cases, however, this may be the only possibility. In the same way, electrons in traps can be directly detected on a phosphor screen on release from the trap.

6. Laser Cooling in the Penning Trap

6.1. *Implementation of Doppler cooling*

We discussed the advantages of using laser-cooled ions in Section 4.4.2 above (see also Chapter 6). Here, we discuss some of the practical aspects of laser cooling as applied in Penning traps and recent progress in cooling ions to their quantum mechanical ground state.

The axial motion of ions in the Penning trap is very similar to that in the RF trap (see Chapter 2), so the same considerations apply. An axial laser cooling beam cools the axial motion directly when it is tuned to the red (low frequency) side of a strong resonance transition in the ion.

The main problem for laser cooling of the radial motion in the Penning trap is the magnetron motion, which does not cool when a cooling laser beam in the radial plane is directed through the center of the trap, as would normally be the case in an RF trap. This is related to the negative total energy of the magnetron motion. Since the total energy of the magnetron motion decreases as the radius of its orbit increases, in general, the interaction with the cooling laser leads to an *increase* of the magnetron radius, not a decrease. Conventional laser cooling with a radial cooling beam therefore heats the magnetron motion while cooling the cyclotron motion (where we define 'cooling' to mean a reduction of radius). The alternative geometry of using just an axial laser beam suffers from a related problem in the same way as resistive cooling, discussed above in Section 4.4.1.

There are several ways of overcoming the problem of cooling the magnetron motion. One is to slightly offset the radial laser cooling beam to the side of the trap so that there is a gradient of laser intensity across the center of the trap. This has the effect of preferentially interacting with the ions when the magnetron motion takes them in the same direction as the laser

beam. If the photon scattering process takes place then, the magnetron motion will on average be cooled (though only slowly in most circumstances) [26,27].

Another way around this problem for a single particle is to couple the magnetron and cyclotron motions using the axialization technique with laser cooling [28] in a similar manner to how it is used for resistive cooling (discussed in Section 4.4.1).

For the laser cooling of clouds of ions rather than single ions, a similar problem arises and relates to the rotation of the plasma discussed above in Section 2.2. In the absence of additional precautions, the plasma expands, its rotation frequency drops towards the magnetron frequency, and its radial extent becomes large, eventually leading to loss of particles. The plasma adopts a strongly oblate shape. This problem is overcome by applying angular momentum to the cloud in one of several ways. The simplest is again to offset the radial laser cooling beam, and this leads to a torque that tends to increase the speed of rotation of the rotating plasma, which then increases in density and adopts a less oblate configuration. Alternatively, a 'rotating wall' potential can be applied. This is an additional radial dipole or quadrupole potential which is applied using a ring electrode that is split into a number of segments. The potentials applied to each segment of the ring electrode are configured such that the generated field rotates around the trap axis at some frequency above the magnetron frequency. The field then slightly distorts the shape of the plasma and forces it to rotate at the applied frequency, thus controlling the plasma density and shape. This technique is discussed in detail in Chapter 11. It is widely used in non-neutral plasma experiments with ions and electrons and it is also routinely applied in combination with laser cooling [29,30].

There is a strong link between the techniques of axialization and the rotating wall. The oscillating quadrupole field of the axialization technique can be decomposed into two quadrupole fields, counter-rotating at half the applied frequency. Ignoring the field rotating in the opposite sense (which is generally justified since it is not resonant with any motion of the ions), the remaining rotating field is the same as that of a quadrupole rotating wall. However, it is most appropriate to think of the rotating wall as a technique for the manipulation of dense non-neutral plasmas in traps, whereas axialization is often more appropriate for a single particle or a small number of particles.

6.2. *Physical picture of Doppler cooling in the Penning trap*

We now describe a physical picture of Doppler cooling that helps in the interpretation of some experiments with laser cooled plasmas and Coulomb crystals in the Penning trap. Conventional laser cooling of neutral atoms can be shown to be equivalent to a damping force acting on the particle under certain approximations. In other words, the force on a particle is always directed against its motion and is proportional to its speed. This is the reason why a set-up with three perpendicular pairs of laser beams for laser cooling of neutral atoms is sometimes known as *optical molasses* because the lasers give rise to a viscous force on the atoms.

In an ion trap, only one beam is required in principle because the ion motion is bound. However, the same reasoning as above applies if the beam runs through the center of the trap. If, however, the laser beam is offset from the center of the trap, this changes the dynamics of the force on the ion. The force can now be shown to correspond to a *rotating* damping force. The frequency of rotation of this force (Ω_0) is proportional to the gradient of the laser intensity across the center of the trap, and it also depends on the detuning of the laser from resonance. It can therefore be varied by changing the laser cooling parameters. For typical cooling parameters, this frequency turns out to be of the order of 100 kHz, i.e. comparable with the magnetron frequency in many experiments [31]. The damping force behaves a bit like a whirlpool, i.e. a viscous fluid that is rotating about some axis. However, in this case, the angular velocity of the rotation is independent of the distance from the origin.

Analysis of the laser beam offset requirements for effective laser cooling [26, 27, 31] shows that a necessary condition is that

$$\omega_m < \Omega_0 < \omega_c'. \tag{7}$$

This means that the rate of rotation of the damping force must fall between the magnetron frequency and the modified cyclotron frequency.

In the rotating frame, this is equivalent to saying that the rate of rotation of the damping force (here equal to $\Omega_0 - \omega_c/2$) must fall between $-\omega_1$ and $+\omega_1$. In a simplified picture, it could be said that the rotating damping force 'tries' to make the ion orbit at the same rate as the damping force. If this is faster (in either the negative or positive sense) than the natural frequency of the simple harmonic well in the rotating frame, then the effect of the force will simply be to drive the particle into ever-increasing orbits, i.e. to heat it. On the other hand, if the rate of rotation of the damping force in this frame is less than the natural frequency of the

potential well, the damping will take it to smaller orbits, which indicates ion cooling.

For a plasma consisting of many ions, the situation is different because it is possible for a plasma to rotate at any frequency between the magnetron frequency and the modified cyclotron frequency (in the laboratory frame), depending on its density. The effect of the rotating damping force is therefore now to force the plasma to rotate at Ω_0, adjusting its density so that this is the equilibrium state. But, if Ω_0 is less than ω_m or greater than ω_c', this cannot be achieved and the plasma will be heated up out of the trap.

6.3. *Demonstration of Doppler cooling*

As an example, we discuss the demonstration of Doppler cooling at Imperial College London. This experiment is carried out using calcium ions, which have the energy level structure shown in Figure 4. The laser cooling transition is at 397 nm, but calcium suffers from the disadvantage that there is a metastable level into which the ions can fall when they decay from the

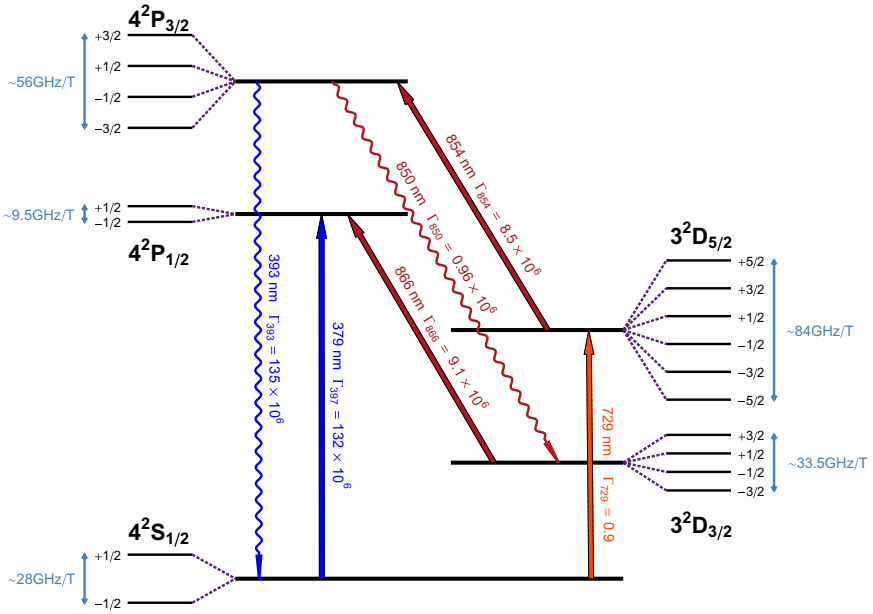

Fig. 4. Energy level diagram for Ca^+. The magnetic field splittings are shown greatly exaggerated. Lasers are required at the wavelengths indicated with solid lines.

$^2P_{1/2}$ excited state. As a result, a separate laser at 866 nm is required, and because of the Zeeman splitting of all levels, laser frequencies addressing all 4 levels of the $^2D_{3/2}$ state as well as both Zeeman levels of the $^2S_{1/2}$ ground state are required.

In this experiment, two sets of Doppler cooling beams are used, one along the trap axis and one in the radial plane so that both axial and radial degrees of freedom (DoF) are strongly cooled. Either the radial beams are offset from the trap axis or an axialization drive is used to ensure that the magnetron motion is cooled.

If the spectrum of a cooled ion is to be recorded by scanning through the resonance transition, there is a problem because as the frequency of the laser cooling beam is changed, the cooling parameters also change, so the temperature of the cooled ion is not constant. In particular, when the laser reaches the line center, it will start laser heating the ion rather than laser cooling it. It can therefore be difficult to interpret the resulting profile as it does not represent a constant temperature. In addition, the natural width of this transition is much larger than the Doppler width at the expected temperature, so it is necessary to deconvolve the Doppler profile from the natural lineshape.

One way around this problem is to record a spectrum of a different transition. In this experiment, the transition from the $^2S_{1/2}$ ground state to the $^2D_{5/2}$ state at 729 nm is recorded. This excited state has a lifetime of around 1 s, so the transition is very narrow and the recorded width represents the Doppler width directly. However, if a narrow laser is used to probe this transition, the lineshape is no longer continuous but consists of a carrier with sidebands (see Figure 5). This is because the ion acts as an oscillator that is frequency modulated at its trap oscillation frequency. For the axial motion, we therefore observe optical sidebands spaced by the axial oscillation frequency (here around 400 kHz). This spectrum demonstrates that the expected Doppler limit temperature of roughly 0.5 mK has been achieved [32]. Although a detailed fit to the quantum dynamics of this spectrum has been used here to determine the temperature, a rough estimate can be obtained simply by measuring the full width at half maximum (FWHM) of the envelope of the observed sideband peaks.

The spectrum of the radial motion is more interesting because it reveals the unusual nature of the motion of an ion in a Penning trap. Such a spectrum is shown in Figure 6. In this spectrum, well-resolved cyclotron sidebands at around 700 kHz can be seen, corresponding to a cyclotron temperature of a few mK. Each cyclotron sideband has structure due to the

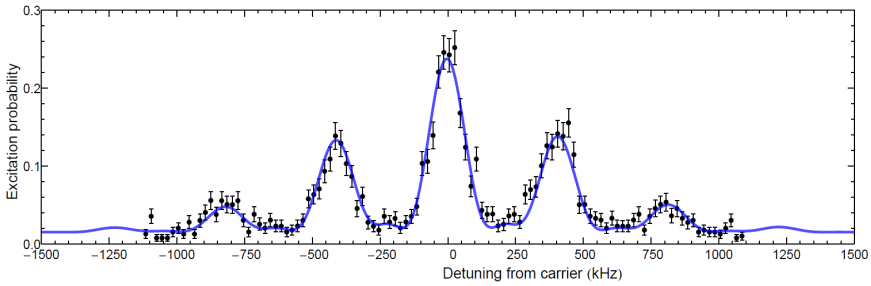

Fig. 5. Optical sideband spectrum of the axial motion of a single ion in a Penning trap after Doppler cooling, recorded at a trap potential of 240 V (giving $\omega_z/2\pi \approx$ 400 kHz). The solid line is a fit to the full quantum dynamics of the system and corresponds to a temperature of $T = 0.47 \pm 0.04$ mK ($\bar{n} = 24 \pm 2$). The error bars reflect the statistical uncertainty in the shelving probability arising from the number of repetitions of the measurement cycle at each frequency step [32].

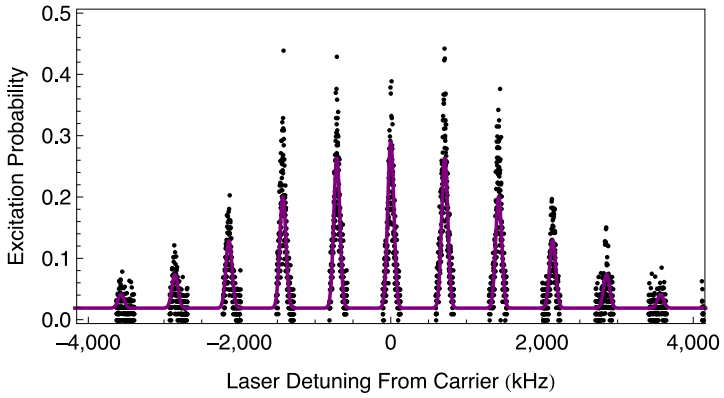

Fig. 6. Radial spectrum showing modified cyclotron sidebands, each of which is broadened due to the magnetron motion. Magnetron sidebands cannot be resolved fully at this trap voltage (5 V) because they are spaced by only 2.5 kHz [32].

magnetron motion, but the sidebands are close together due to the small value of the magnetron frequency, and are therefore unresolved. However, it is clear that the magnetron sidebands have an overall width of only a few tens of kHz, which implies a temperature of only a few tens of μK, much less than the standard Doppler limit. This counter-intuitive result is not unexpected and follows from the fact that the magnetron motion is only cooled very slowly as a result of the laser beam offset discussed above.

Its Doppler limit is therefore much lower than that of the cyclotron motion, which is cooled strongly and has roughly the standard value [32].

6.4. *Optical sideband cooling*

Optical sideband cooling is discussed in Chapter 6. It is best to think of this in terms of the ladder of equally spaced energy levels of the quantum mechanical simple harmonic oscillator represented by the axial motion of the ion in the quadratic trap potential. The steps of the ladder are spectroscopically resolved if they are probed on a narrow optical transition with a highly-stabilized laser. The 729 nm transition, used for the spectroscopic results shown in Figures 5 and 6, is very suitable for this. In sideband cooling, an excitation on the first sideband on the low frequency side of the carrier transition (the 'red sideband') lowers the quantum simple harmonic oscillator state quantum number n by 1 each time the ion is excited. On decay, it is most likely to stay in the same state, so each complete cycle on average lowers the quantum number by 1, and eventually the ion should end up in the ground state ($n = 0$). The sign of this is that the red sideband then disappears because there is no state with a lower value of n that can be excited. This can be seen clearly in Figure 7 which shows the first red and blue sidebands after sideband cooling.

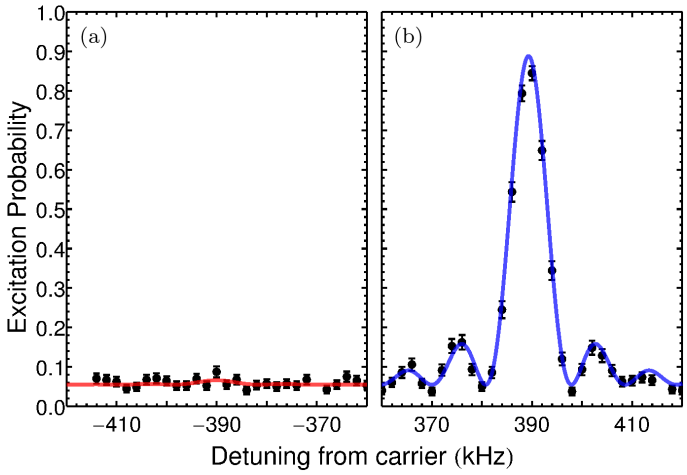

Fig. 7. (a) First red and (b) first blue sidebands after 21 ms of sideband cooling on the first red sideband of the axial motion. The ratio of the sideband heights above the background shows that the average photon number is $\bar{n} = 0.013 \pm 0.009$ [33]. Each plot shows the measured data as points and the fit to the expected coherent dynamics as a solid line.

6.5. *Coulomb crystals*

A striking consequence of the powerful technique of laser cooling is the creation of *ion Coulomb crystals* (ICC) (see Chapter 15). These structures appear when the temperature of a cloud of ions is so low that the Coulomb interaction between particles overcomes thermal effects. The result of this is that the particles form a regular crystal-like structure where the ions have fixed positions relative to each other. The equilibrium distance between particles is determined by a balance between their mutual Coulomb repulsion and the trapping force which pushes them together. Since this distance is typically tens of μm in a Penning trap, the density of such a crystal is many orders of magnitude lower than that of a conventional crystal — in fact, it is usually lower than the density of the residual gas in the vacuum chamber.

Ion Coulomb crystals can be created in both Penning and RF traps [34]. The configuration of an ICC is dependent on the strength of the axial and radial confinement. For very low axial confinement, the equilibrium configuration is a string of ions along the axis of the trap. This type of structure is used for experiments such as quantum information processing in linear RF traps (e.g. [35]). For intermediate ratios of the axial to radial confinement strength, ellipsoidal crystals are formed, and these have been used for a wide range of applications including, for example, cavity QED [36] and the study of ion processes such as ionization and charge exchange [37]. When the radial confinement is weak, crystals can adopt a planar configuration. This is not generally used in linear RF traps because there is a driven *micromotion* for any particles that are not located on the axis of the trap and this becomes much more significant as the radial extent of the crystal increases.

ICC were first observed in Penning traps by the Boulder group [39] and their structure was investigated by direct imaging and also by using Bragg scattering [40]. This group has worked extensively with planar crystals in a Penning trap and has used these for the study of the *drumhead* modes of oscillation of the crystal [41] and for quantum simulation of 2D Ising interactions [38]. An image of such a crystal (as viewed along the axis of the trap) is shown in Figure 8. Since the ion cloud in a Penning trap always rotates around the trap axis, whether it is in the form of a plasma or a crystal, each ion is executing an orbit around this axis. In Figure 8, this is overcome by imaging the crystal with a position-sensitive photomultiplier tube so that the position as well as the time of arrival of each photon is known. Since the rotation frequency of the crystal is also known (because it is driven using the rotating wall technique discussed in Section 6.1), the

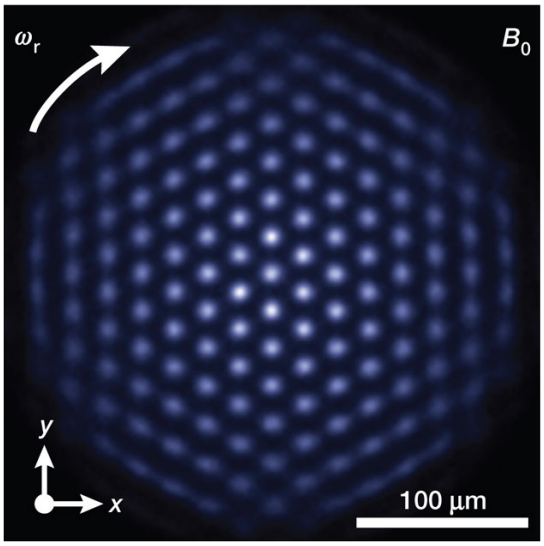

Fig. 8. An image of an ion Coulomb crystal consisting of a single plane of Be^+ ions in a Penning trap [38]. The crystal is rotating, but the image is reconstructed using timing information from a position-sensitive photomultiplier. Reprinted by permission from Macmillan Publishers Ltd: *Nature* **484**, 489, copyright 2012.

rotation of the crystal can effectively be frozen out, so the ions are imaged as points.

The whole range of configurations of a small crystal in a Penning trap, in this case containing 15 ions, can be seen in Figure 9. The ions are imaged here from a direction perpendicular to the trap axis, so the image of each ion is averaged over its radial motion and becomes a horizontal line. The only parameter which is changed between all these images is the trapping potential which ranges in this figure from 10% to 85% of the maximum value it can take for stable trapping.

As explained above, in a Penning trap, the plasma (or in this case, the crystal) is always rotating, and in the presence of laser cooling with a radially offset cooling beam, the speed of rotation is determined by the value of Ω_0, i.e. the rate of rotation of the damping force arising from the laser cooling beam (see Section 6.2). This in turn determines the density of the crystal through Equation (4), and also its aspect ratio (i.e. the ratio of the length to the diameter of the crystal). In the examples shown in Figure 9, each pane shows the experimentally obtained image on the left and a simulated image on the right. This simulated image takes into account the known

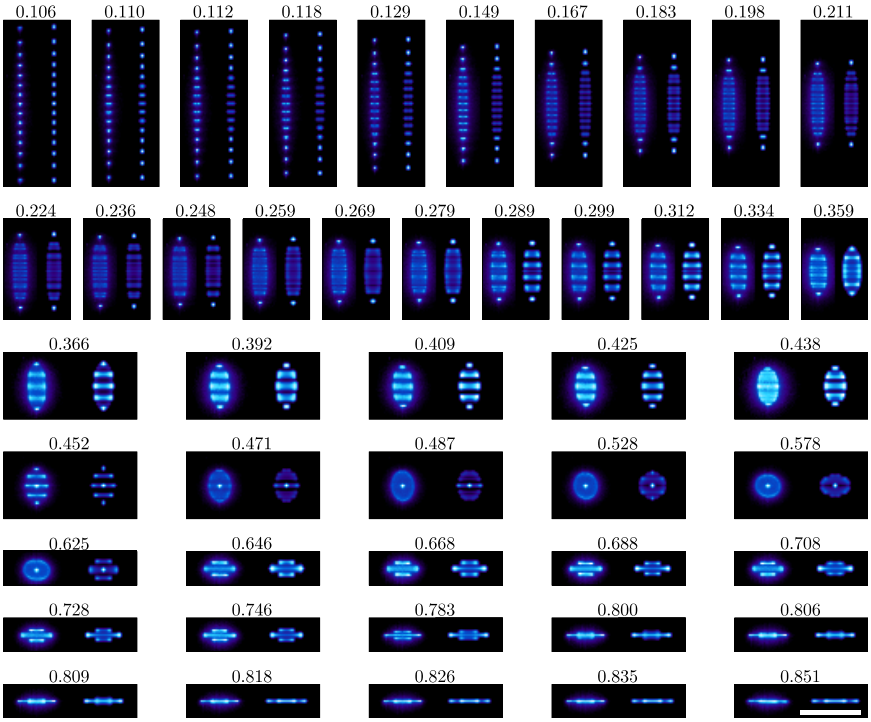

Fig. 9. Conformations of a 15-ion crystal in a Penning trap [42]. Experimentally obtained images (left side of each pane) are compared to computer simulations (right side of each pane). By increasing the axial confinement, a linear string is transformed into a zigzag structure, then a 3-D crystal and finally a planar structure. Each image is labeled with the value of the normalized axial trapping frequency, which increases with the trapping voltage (the trap becomes unstable when this quantity is equal to unity). There is a 100 μm scale bar in the bottom right-hand pane which applies to all the images. Reprinted by permission from Macmillan Publishers Ltd: *Nature Communications* **4**, 2571, copyright 2013.

trapping voltage and is matched by eye to the experimental image only by varying the rate of rotation of the crystal in the simulation. This allows the rate of rotation of the crystal to be determined from the best match of the simulated image to the real image. As expected, this turns out to be consistent with the value of Ω_0 estimated from the parameters of the laser cooling beam, and is found to be roughly constant for all the images in the figure, demonstrating that the crystal rotation always matches the rotation of the damping force created by the laser cooling beam, independent of the crystal configuration [42].

7. Conclusions

Penning traps are now well established in many areas of pure and applied science as powerful and versatile devices for carrying out experiments that in many cases would not otherwise be possible. In this chapter, we have set out the basic principles of how Penning traps work and illustrated some of their properties by discussing a few examples of their applications. We have not attempted to present a comprehensive review of their many uses but rather to give an understanding of their basic properties so that the reader can then investigate specific applications in more detail.

When it was first discovered more than 50 years ago that there was a configuration of static electric and magnetic fields that would lead to stable trapping of charged particles in a vacuum, it could not have been anticipated that this fact could be exploited in so many different situations, with applications ranging from fundamental physics topics such as the simulation of interacting quantum spins and the creation of antimatter, to practical uses such as routine mass spectrometry. Even now, it is not possible to say what other applications could be found in the future for particles held in a Penning trap.

8. Problem Set

Question 1

Starting from the Lorentz force on a charged particle in static electric (**E**) and magnetic (**B**) fields,

$$\mathbf{F} = e(\mathbf{E} + v \times \mathbf{B}) \tag{8}$$

with an electrostatic potential

$$\phi(r) = A(2z^2 - x^2 - y^2), \tag{9}$$

find the three oscillation frequencies (ω_z, ω_c, and ω_m) for a singly charged calcium ion in a magnetic field of 1 T and with $A = 1 \times 10^5$ Vm^{-2}.

Also, find the frequencies for the case of an electron in the same fields.

Question 2

Consider two stationary calcium ions located on the z-axis of the trap in Question 1, at positions $+z_1$ and $-z_1$. By equating the confining force from the trap with the Coulomb repulsion, find the equilibrium value of z_1.

Question 3

Thinking of an ion in the above trap as a quantum mechanical simple harmonic oscillator, calculate the "width" of the ground state wave function for the axial motion. [If you do not remember the formula for this, you can estimate it by calculating the amplitude of the classical motion of an ion having the zero-point energy $\hbar\omega_z/2$.]

Comparing the results of Questions 2 and 3, do you think it is possible to observe effects due to the overlap of ground state ion wavefunctions in a trap?

Question 4

In the book *Angels and Demons*, Dan Brown imagines a device that sounds similar to a Penning trap but stores enough liquid antihydrogen to destroy the Vatican. Imagine instead a real Penning trap (with a 1 T field) containing 1 cm^3 of antiprotons at the maximum possible density (i.e. at the Brillouin limit). What is the number density of antiprotons and how much energy would be released if the antiprotons were allowed to annihilate?

Question 1 solution

The force is

$$\mathbf{F} = e(\mathbf{E} + v \times \mathbf{B}), \tag{10}$$

but $\mathbf{E} = -\nabla\phi$ and $\phi = A(2z^2 - x^2 - y^2)$, so this gives

$$\mathbf{E} = 2Ax\hat{\mathbf{x}} + 2Ay\hat{\mathbf{y}} - 4Az\hat{\mathbf{z}} \tag{11}$$

and $\mathbf{v} \times \mathbf{B} = \dot{y}B\hat{\mathbf{x}} - \dot{x}B\hat{\mathbf{y}}$, so

$$m\ddot{\mathbf{r}} = \mathbf{F} = e[(2Ax + \dot{y}B)\hat{\mathbf{x}} + (2Ay - \dot{x}B)\hat{\mathbf{y}} - 4Az\hat{\mathbf{z}}]. \tag{12}$$

Writing $\omega_c = eB/m$ and $\omega_z^2 = 4eA/m$, we find

$$\ddot{x} - \omega_c\dot{y} - (\omega_z^2/2)x = 0, \tag{13}$$

$$\ddot{y} + \omega_c\dot{x} - (\omega_z^2/2)y = 0, \tag{14}$$

$$\ddot{z} + \omega_z^2 z = 0. \tag{15}$$

The solutions are of the form $C \exp i\omega t$ and Equations (13) and (14) give for the two components of the radial motion,

$$\omega = \omega_c' = \omega_c/2 + \sqrt{\omega_c^2/4 - \omega_z^2/2}, \tag{16}$$

$$\omega = \omega_m = \omega_c/2 - \sqrt{\omega_c^2/4 - \omega_z^2/2}. \tag{17}$$

Equation (15) gives $\omega = \omega_z$ for the axial motion. Putting in the values of $\mathbf{B}$ = 1 T and $A = 1 \times 10^5$ Vm^{-2}, we find (for $^{40}Ca^+$) $\omega_c = 2.4 \times 10^6$ s^{-1} [380 kHz], $\omega_z = 9.8 \times 10^5$ s^{-1} [156 kHz], $\omega_c' = 2.2 \times 10^6$ s^{-1} [346 kHz] and $\omega_m = 2.4 \times 10^5$ s^{-1} [35 kHz].

For electrons, we find $\omega_c = 1.76 \times 10^{11}$ s^{-1} [28 GHz], $\omega_z = 2.65 \times 10^8$ s^{-1} [42 MHz], $\omega_c' = 1.76 \times 10^{11}$ s^{-1} [28 GHz] and $\omega_m = 2.0 \times 10^5$ s^{-1} [32 kHz]. Note that ω_m is nearly the same for both species despite the large mass difference.

Question 2 solution

The two particles sit on the z-axis displaced from the origin by equal and opposite amounts. The inwards force on each particle is $mz_1\omega_z^2$ and the outwards force on each particle is $e^2/4\pi\epsilon_0(2z_1)^2$, so in equilibrium, we find

$$mz_1\omega_z^2 = e^2/4\pi\epsilon_0 z_1^2, \tag{18}$$

which gives $z_1^3 = e^2/16\pi\epsilon_0 m\omega_z^2$. For $^{40}Ca^+$, we find $z_1 = 10.1$ μm (for the trap parameters given above). The separation of the particles is therefore just over 20 μm.

Question 3 solution

We can use two different approaches to get a rough estimate. The uncertainty principle says that $\Delta z \Delta p_z \sim (z_0)(m\omega_z z_0) \sim \hbar$, where z_0 represents the approximate size of the ground state wave function. From this, we find $z_0 = \sqrt{\hbar/m\omega_z} = 0.04\,\mu$m. Alternatively, we get the same result by equating the ground state energy $\frac{1}{2}\hbar\omega_z$ to the potential energy $\frac{1}{2}m\omega_z^2 z_0^2$.

Comparing this result with the typical separation of ions derived in Question 2, we can see that under normal circumstances, the wavefunctions are well separated, so we expect no effects due to wavefunction overlap. However, it is possble to engineer situations where there are two different structural configuations of an ion Coulomb crystal that only involve very small displacements of the ions when the configuration changes. Under these circumstances, it is possible in principle to see quantum mechanical

effects, though they are technically very challenging to observe. An example is a string of ions having an equilibrium configuration that is very slightly kinked to the left or the right. The wavefunctions of the whole system can have some overlap, so the state with the system in either one or the other configuration is no longer an eigenstate of the system and quantum tunnelling between the two configurations could be observed.

Question 4 solution

With $B = 1$ T, the maximum density of particles is $n = \epsilon_0 B^2/2m = 6.6 \times 10^{13}$ m^{-3}. So 1 cm^3 contains 66 million antiprotons, each of which has a rest mass energy of mc^2, giving a total energy of 0.4 J. It is also interesting to note that the same value can be obtained by calculating the energy density of the magnetic field, $B^2/2\mu_0$, multiplied by the volume of the cloud.

Acknowledgments

This work was supported in part by the European Commission STREP PICC (FP7 2007–2013 Grant number. 249958). We also gratefully acknowledge financial support toward networking activities from COST Action MP 1001 — Ion Traps for Tomorrows Applications.

References

1. H. Dehmelt, Radiofrequency spectroscopy of stored ions I: Storage, *Advances in Atomic and Molecular Physics*, Vol. 3, pp. 53–72. New York, Academic Press (1968).
2. H. Dehmelt, Radiofrequency spectroscopy of stored ions II: Spectroscopy. vol. 5, *Advances in Atomic and Molecular Physics*, pp. 109–154. New York, Academic Press (1969).
3. H. Dehmelt, Experiments with an isolated subatomic particle at rest (Nobel Lecture), *Angew. Chem. Int. Ed. Engl.* **29**(7), 734–738 (1990).
4. F. Penning, Die Glimmentladung bei niedrigem Druck zwischen koaxialen Zylindern in einem axialen Magnetfeld, *Physica* **3**(9), 873–894 (1936).
5. H. G. Dehmelt and F. L. Walls, "Bolometric" technique for the RF spectroscopy of stored ions, *Phys. Rev. Lett.* **21**, 127–131 (1968).
6. J. Byrne and P. S. Farago, On the production of polarized electron beams by spin exchange collisions, *Proc. Phys. Soc.* **86**(4), 801 (1965).
7. G. Gräff *et al.*, Method for measuring the cyclotron and spin resonance of free electrons, *Phys. Rev. Lett.* **21**, 340–342 (1968).
8. G. Gräff *et al.*, Method for measuring the anomalous magnetic moment of free electrons, *Zeitschrift für Physik*. **222**(3), 201–207 (1969).

9. D. J. Wineland *et al.*, Radiation-pressure cooling of bound resonant absorbers, *Phys. Rev. Lett.* **40**, 1639–1642 (1978).
10. L. S. Brown and G. Gabrielse, Geonium theory — physics of a single electron or ion in a Penning trap, *Rev. Modern Phys.* **58**(1), 233–311 (1986).
11. R. C. Thompson and D. C. Wilson, The motion of small numbers of ions in a Penning trap, *Zeitschrift Fur Physik D-Atoms Molecules and Clusters.* **42**(4), 271–277 (1997).
12. J. Bollinger *et al.*, 303-MHz frequency standard based on trapped Be^+ ions, *IEEE Transactions on Instrumentation and Measurement.* **40**(2), 126–128 (1991).
13. M. Mukherjee *et al.*, ISOLTRAP: An on-line Penning trap for mass spectrometry on short-lived nuclides, *Eur. Phys. J. A.* **35**(1), 1–29 (2008).
14. A. Solders *et al.*, Determination of the proton mass from a measurement of the cyclotron frequencies of D^+ and H_2^+ in a Penning trap, *Phys. Rev. A.* **78**, 012514 (2008).
15. A. G. Marshall *et al.*, Fourier transform ion cyclotron resonance mass spectrometry: A primer, *Mass Spectrom. Rev.* **17**(1), 1–35 (1998).
16. D. Hanneke *et al.*, New measurement of the electron magnetic moment and the fine structure constant, *Phys. Rev. Lett.* **100**, 120801 (2008).
17. A. Mooser *et al.*, Direct high-precision measurement of the magnetic moment of the proton, *Nature* **509**(7502), 596–599 (2014).
18. J. DiSciacca *et al.*, One-particle measurement of the antiproton magnetic moment, *Phys. Rev. Lett.* **110**, 130801 (2013).
19. J. Verdú *et al.*, The magnetic moment anomaly of the electron bound in hydrogen-like oxygen $^{16}O^{7+}$, *J. Phys. B: At. Mol. Opt. Phys.* **36**(3), 655 (2003).
20. W. Quint *et al.*, Laser-microwave double-resonance technique for g-factor measurements in highly charged ions, *Phys. Rev. A.* **78**, 032517 (2008).
21. C. Lichtenberg *et al.*, Axialisation, cooling and quenching of ions in a Penning trap, *Eur. Phys. J. D: At. Mol. Opt. Plasma Phys.* **2**(1), 29–32 (1998).
22. D. M. Segal and C. Wunderlich, *Physics with Trapped Charged Particles (Eds M. Knoop, N. Madsen and R. C. Thompson)*, Chapter 3 Cooling Techniques for Trapped Ions, pp. 43–81. London, Imperial College Press (2014).
23. M. A. van Eijkelenborg *et al.*, Sympathetic cooling and detection of molecular ions in a Penning trap, *Phys. Rev. A.* **60**, 3903–3910 (1999).
24. G. Gabrielse *et al.*, Open-endcap Penning traps for high precision experiments, *Int. J. Mass Spectrom. Ion Process.* **88**(2–3), 319–332 (1989).
25. M. Knoop, *Physics with Trapped Charged Particles (Eds M. Knoop, N. Madsen, and R. C. Thompson)*, Chapter 2 Detection Techniques for Trapped Ions, pp. 25–42. London, Imperial College Press (2014).
26. W. M. Itano and D. J. Wineland, Laser cooling of ions stored in harmonic and Penning traps, *Phys. Rev. A.* **25**, 35–54 (1982).
27. R. C. Thompson and J. Papadimitriou, Simple model for the laser cooling of an ion in a Penning trap, *J. Phys. B: At. Mol. Opt. Phys.* **33**(17), 3393–3405 (2000).
28. H. F. Powell *et al.*, Axialization of laser cooled magnesium ions in a Penning trap, *Phys. Rev. Lett.* **89**, 093003 (2002).
29. X. P. Huang *et al.*, Phase-locked rotation of crystallized non-neutral plasmas by rotating electric fields, *Phys. Rev. Lett.* **80**(1), 73–76 (1998).

30. S. Bharadia *et al.*, Dynamics of laser-cooled Ca^+ ions in a Penning trap with a rotating wall, *Appl. Phys. B: Lasers O.* **107**(4), 1105–1115 (2012).
31. M. Asprusten *et al.*, Theory and simulation of ion Coulomb crystal formation in a Penning trap, *Appl. Phys. B: Lasers O.* **114**(1–2), 157–166 (2014).
32. S. Mavadia *et al.*, Optical sideband spectroscopy of a single ion in a Penning trap, *Phys. Rev. A.* **89**, 032502 (2014).
33. J. G. Goodwin. *Sideband Cooling to the Quantum Ground State in a Penning Trap.* PhD thesis, Imperial College London (2015).
34. R. C. Thompson, Ion Coulomb crystals, *Contemp. Phys.* **56**, 63–79 (2015).
35. T. Monz *et al.*, 14-qubit entanglement: Creation and coherence, *Phys. Rev. Lett.* **106**, 130506 (2011).
36. A. Dantan *et al.*, Large ion Coulomb crystals: A near-ideal medium for coupling optical cavity modes to matter, *Phys. Rev. A.* **80**(4), 4 (2009).
37. M. Drewsen *et al.*, Ion Coulomb crystals: a tool for studying ion processes, *Int. J. Mass Spectrom.* **229**(1–2), 83–91 (2003).
38. J. W. Britton *et al.*, Engineered 2D Ising interactions in a trapped-ion quantum simulator with hundreds of spins, *Nature* **484**(7395), 489–492 (2012).
39. S. L. Gilbert *et al.*, Shell-structure phase of magnetically confined strongly coupled plasmas, *Phys. Rev. Lett.* **60**, 2022–2025 (1988).
40. J. N. Tan *et al.*, Long-range order in laser-cooled, atomic-ion Wigner crystals observed by Bragg scattering, *Phys. Rev. Lett.* **75**(23), 4198–4201 (1995).
41. B. C. Sawyer *et al.*, Spectroscopy and thermometry of drumhead modes in a mesoscopic trapped-ion crystal using entanglement, *Phys. Rev. Lett.* **108**(21), 213003 (2012).
42. S. Mavadia *et al.*, Control of the conformations of ion Coulomb crystals in a Penning trap, *Nat. Commun.* **4**, 2571 (2013).